RSC Advances

ROYAL SOCIETY OF CHEMISTRY

www.rsc.org/advances

Dimethyl Carbonate Synthesis from Carbon Dioxide and Methanol over CeO_2 and ZrO_2: Comparison of Mechanism

Lei Chen, Shengping Wang*, Jingjie Zhou,Yongli Shen, Yujun Zhao, Xinbin Ma

Key Laboratory for Green Chemical Technology, School of Chemical Engineering and Technology, Tianjin University; Collaborative Innovation Center of Chemical Science and Engineering, Tianjin 300072, China

* Corresponding author

E-mail address: spwang@tju.edu.cn

Telephone: +86-22-87401818

Fax: +86-22-87401818

Abstract:

The comparison of mechanism of dimethyl carbonate (DMC) formation directly from carbon dioxide and methanol over CeO_2 and ZrO_2 is investigated through *in-situ* fourier transform infrared spectroscopy (FTIR). A new band around 1295 cm^{-1} appears during the methanol and CO_2 adsorption over CeO_2. Connected with the *in-situ* FTIR results of methyl formate adsorption, this band is assigned to carbomethoxide, which is taken as the intermediate in DMC formation over ceria surface. Carbomethoxide comes from the reaction of methanol and adsorbed carbon dioxide, followed by the reaction with methoxy to form DMC. This mechanism differs with that obtained on zirconium oxide, from which DMC is formed by the reaction between monodentate methyl carbonate with methanol.

Key words: dimethyl carbonate; carbomethoxide; monodentate methyl carbonate; *in situ* Fourier Transform Infrared Spectroscopy; CeO_2; ZrO_2

Introduction

As a new carbon source, carbon dioxide conversion has been increasingly attracting great interests due to the worries about the global warming and sustainable development of society. There are several strategies about CO_2 utilization [1-4]. Among these ways, dimethyl carbonate (DMC), which has been widely application in the industrial process such as fuel additive, methylation agent and solvent, direct synthesis from CO_2 and methanol is a promising approach. Converting CO_2 into environmentally friendly compounds can not only relieve the greenhouse damages, but can also take CO_2 as a new carbon source alternative to coal, natural gas and petroleum.

Both homogeneous and heterogeneous catalysts have been applied in this reaction system [5-9]. Zirconium oxide has been proved to be a useful heterogeneous catalyst, on which the mechanism of DMC formation is well studied based on the acidic and basic properties [10]. In recent years, cerium oxide is applied to many fields [11,12] and also demonstrated to be an effective catalyst in DMC formation due to the acidity and basicity on catalyst surface. [8,13]. However, the present mechanism of DMC formation on ceria is almost referred to that on zirconium oxide in the absence of the comprehensive investigation [8,14], which is not favorable for further modifying catalyst surface and enhancing the catalytic activity. Recently, CeO_2 has been attracting interest for its high oxygen storage capacity in CO_2 activation. And some researchers [15,16] have confirmed that CO_2 can be activated on ceria surface. It will be helpful in DMC formation if CO_2 can be activated more easily. When CO_2 activation is involved in the mechanism, the elementary steps should be different from that on zirconium. However, most researchers do not take this into account when they present the mechanism on ceria catalyst [8,14].

In this paper, CeO_2 and ZrO_2 are prepared by sol-gel method. *In-situ* Fourier Transform Infrared Spectroscopy (FTIR) is applied to track each reaction steps to figure out the difference in the mechanism between ceria catalyst and zirconium oxide.

Experimental Design

Catalyst preparation:

The CeO_2 and ZrO_2 were prepared by sol-gel method with $Ce(NO_3)_3 \cdot 6H_2O$ and $Zr(NO_3)_4 \cdot 4H_2O$ as precursors. 5.211g $Ce(NO_3)_3 \cdot 6H_2O$ or 1.288g $Zr(NO_3)_4 \cdot 4H_2O$ was dissolved in 50 ml deionized water, respectively. Then the solution was transferred into a 250 ml beaker and 5.04 or 1.26 g citric acid was added into the cerium or zirconium solution, respectively. The mixed solution was stirred for 3h under 353K, then vaporized at the same temperature to remove the water until a sol obtained. The sol was dried at 373 K overnight and then calcinated at 873 K for 5 h.

Catalytic test

The direct formation of DMC from CO_2 and methanol was carried out in an autoclave. 0.1 g catalyst and 15 ml CH_3OH were put into the autoclave. The reactor was pressurized with 5 MPa CO_2. Then the reactor was heated to 413 K and stirred for 2 h. 1-propanol as an internal standard substance was added to quantify the mixture. Products were analyzed with a gas chromatograph (GC, Agilent 4890 D).

Catalyst characterization

X-ray diffraction was measured with a Rigaku D/max 2500 diffractometer equipped with a Cu Kα radiation in a diffraction angle ranging from 10 to 90° with a scanning rate of 8°/min.

In-situ FTIR was carried out by a Nicolet spectrometer with an MCT detector. 4 scans were averaged with a resolution of 4 cm^{-1}. Before the experiment, the samples were pressed into a disc

and transferred to a homemade reaction cell which uses the ZnSe windows. Temperature of cell was controlled with a programmable temperature controller.

The disc was pretreated under He stream at 673 K for 1h. Then the sample was cooled to reaction temperature in He stream before exposed to reactant stream. The entire process was conducted at 0.1 MPa. The flow rate of He and CO_2 were 15 ml/min and 10 ml/min, respectively. He stream passed through drying agent to remove water and was deoxidized in deoxidizing tube. DMC, methanol, formic acid and methyl formate were introduced into the reaction unit by He stream through a bubbling sampler which was maintained at 298 K.

Results

Table.1 shows the catalytic activity of CeO_2 and ZrO_2 for synthesis of DMC from CO_2 and methanol. DMC is the only product under the experiment condition. It can be clearly seen that the CeO_2 exhibit a more favorable activity in DMC synthesis than ZrO_2, which is consistent with the results of other researchers [17, 18].

Fig. 1 exhibits the XRD patterns of CeO_2 and ZrO_2 catalysts. As shown in Fig. 1(a), diffraction peaks at 2θ=28.6°, 33.1°, 47.6° and 56.4° are associated with cubic fluorite phase of CeO_2, corresponding to the planes of (111), (200), (220) and (311), respectively. For Fig. 1(b), diffractions at 2θ=28.2° and 31.5° are assigned to monoclinic phase of ZrO_2. Peak at 2θ = 30.2° is attributed to the tetragonal phase of ZrO_2. This means that ZrO_2 is the mix of monoclinic and tetragonal phases, which accords with the result of Parghi[19]. There are no other diffraction peaks in ZrO_2 or CeO_2, indicating that ZrO_2 and CeO_2 are both in high purity.

Fig. 2 shows the IR spectra of methanol adsorption on ceria catalysts. Methanol interacts with ceria catalysts surface through the oxygen atoms. Features for ν(CO) of methoxy grow simultaneously at 1097, 1054 and 1012 cm^{-1}, attributed to on-top methoxy, bridging methoxy and three coordinate methoxy, respectively [20]. The intensity of on-top methoxy rises much

slower than that of others. The band around 1031 cm^{-1} may be ascribed to bridging methoxy or physisorbed methoxy. In $\nu(CH_3)$ region, there are two types of vibration: bands at 2806 and 2915 cm^{-1} are associated with the modes of $\nu(CH_3)$ and $\nu_{as}(CH_3)$ of chemisorbed methoxy; 2834 and 2934 cm^{-1} are attributed to symmetric and asymmetric CH_3 stretching modes of physisorbed methanol. Bands which are observed at 1575, 1453 and 1369 cm^{-1} represent monodentate methyl carbonate (MMC). Band around 1295 cm^{-1} which has not been assigned so far also emerges. Fig. 3 shows the spectra of successive methanol adsorption on ZrO_2 surface, which is identical with the results of other researchers [21] except the intensity. Bands at 1162 and 1032 cm^{-1} are associated with the bending vibration of methoxy groups and the bands at 2822 and 2924 cm^{-1} with the increasing intensity are ascribed to the C-H stretching vibration of bidentate and monodentate methoxy. The decreasing absorbance of bands (3768, 3686, and 3674 cm^{-1}) are associated with different types of OH groups on the ZrO_2 surface [22].

Exposure of ceria catalysts containing preadsorbed methanol to CO_2 stream leads to a remarkable change in the infrared spectra. As seen in Fig. 4, band representing on-top methoxy decreases, but the features for MMC (1574, 1457 and 1374 cm^{-1}) increase. The band at 1295 cm^{-1} also experience increase, although it does not have a specific assignment. Band at 1468 and 1356 cm^{-1} are associated with monodentate carbonate. Peak at 1549 and 1018 cm^{-1} indicate the appearance of bidentate carbonate [23, 24]. Infrared spectra taken during exposure of ZrO_2 containing preadsorbed methanol to CO_2 are shown in Fig. 5. Bands for on-top and bridging methoxy (1158 and 1032 cm^{-1}) decrease and new peaks appear at 1596, 1497, 1471, 1391, 1362, 1200 and 1110 cm^{-1} which are ascribed to MMC [10]. The formation of MMC can also be confirmed through the C-H stretching vibration. Bands (2924 and 2818 cm^{-1}) for methoxy species decrease while new bands at 2960 and 2880 cm^{-1} appear [10]. The peak around 1295 cm^{-1} does not appear during this process.

Fig. 6 exhibits infrared spectra recorded the adsorption of CO_2 on CeO_2. The bands for $\nu_{as}(CO_2)$ in gas phase are clearly observed at 2358 and 2340 cm^{-1}. Bands at 1560, 1289 and 1011 cm^{-1} stem from $\nu(CO_3)$ of bidentate carbonate [23, 24], while 1467, 1352 and 1088cm^{-1} are features for $\nu(CO_3)$ of monodentate carbonate [23, 25]. Peaks at 1598 and 1413 cm^{-1} are ascribed to hydrogen carbonate [23, 26]. Spectra of ZrO_2 reacting with CO_2 at 413 K are shown in Fig. 7. The clear bands at 1221, 1425, 1626 and 1683 cm^{-1} are assigned to bicarbonate, and 1366 cm^{-1} may indicate the presence of bidentate carbonate [27].

Fig. 8 displays the spectra of methanol successive introduction to CeO_2 after CO_2 adsorption. Peaks in $\nu(CH_3)$ and $\nu(CO)$ region representing different kinds of methoxy all appear. New weak bands at 1572, 1454 and 1369 cm^{-1} are assigned to MMC. The unassigned band at 1295 cm^{-1} rise, too. Features (1602 and 1410 cm^{-1}) for hydrogen carbonate decrease in methanol stream. Intensity of bands (1463 and 1354 cm^{-1}) for monodentate carbonate reduces, too. Fig. 9 illustrates the transformation of spectra when methanol starts to adsorb on ZrO_2 containing preadsorbed CO_2. New bands appearing at 1165 and 1033 cm^{-1} are for top- and bridging-methoxy, respectively. Features for 1605, 1463 and 1354 cm^{-1} are associated with MMC [28]. There is no sign around 1295 cm^{-1} during the CO_2 adsorption process.

Fig. 10 shows the infrared spectra of DMC adsorbed on ceria catalysts. In the $\nu(CH_3)$ region, bands at 2910 and 2804 cm^{-1} increase in intensity with time, which are assigned to $\nu_{as}(CH_3)$ and $\nu_s(CH_3)$ of methoxy, respectively. 2965 and 2869 cm^{-1} are associated with the $\nu_{as}(CH_3)$ and $\nu_s(CH_3)$ of DMC. Bands at 1780 and 1767 cm^{-1} may relate with the physisorbed DMC because these bands can be totally removed when the sample is exposed in pure He stream. Features at 1109 and 1061 cm^{-1} are associated with the $\nu(CO)$ of on-top methoxy and bridging methoxy. The unassigned peak around 1295 cm^{-1} with a great increase appears, too. Fig. 11 records the infrared spectra of DMC passing over ZrO_2. Bands at 1603, 1357 and 1200

cm^{-1} indicate the appearance of MMC on zirconium [28]. The on-top methoxy is evident with the rising band at 1166 cm^{-1}. Other types of methoxy also appear during DMC adsorption process.

Fig. 12 illustrates the transformation of infrared spectra when CeO_2 is exposed to HCOOH in He stream. The bands are ascribed to formate species [23], i.e., ν(C-H), 2842 cm^{-1}, ν_{as}(OCO), 1590, 1557, δ(C-H), 1371 cm^{-1}, ν_s(OCO), 1353, 1252 cm^{-1}. Peak at 2925 cm^{-1} results from the combination band of ν_{as}(OCO) and δ(C-H) [29]. It has been indicated that the frequency differences between ν_{as}(OCO) with ν_s(OCO) keep the following sequence: monodentate formate > free formate ion > bidentate formate. According to this empirical approach, bands at 1590 and 1252 cm^{-1} may result from the monodentate formate because the frequency separation is 338 cm^{-1}, which is much larger than 250 cm^{-1} of free formate ion. The remaining features (1557, 1353 cm^{-1}) are associated with the bidentate formate since the frequency separation is 204 cm^{-1} smaller than 250 cm^{-1}. During the adsorption process, there is no sign about the peak around 1295 cm^{-1}.

The spectra of methyl formate adsorption on ceria catalysts evolve in a complicated way. Bands observed at 3040, 3008, 2967, 2947, 1766 and 1753 cm^{-1} in Fig. 13 are assigned to methyl formate physisorbed on cerium oxide [30]. The peak at 2926 cm^{-1} is associated with the combination band of ν_{as}(OCO) and δ(C-H). Bands at 2844, 1599, 1559, 1377, 1353 and 1248 cm^{-1} are due to the formate adsorbed on surface. A shoulder at 2915 and 2801 cm^{-1} are similar with those peaks which result from the exposure of ceria catalysts to methanol. In the region of ν(CO), bands at 1032 and 1020 cm^{-1} are associated with the bridging and tri-coordinate methoxy. It is worth mentioning that band around 1295 cm^{-1} appears as expected.

Discussion

The spectra of methanol adsorption on ceria and zirconium [10, 20, 31] are shown in Fig. 2 and Fig. 3. It is indicated that CH_3OH adsorbs on these two catalysts through O atom. The H atom of

hydroxyl in methanol can react with the OH on metal oxide surface or a coordinately unsaturated O^{2-} on the surface to produce hydroxyl. The negative going features of ν(OH) in Fig. 3 indicate that the H atom combines with the OH to produce H_2O on ZrO_2 surface. However, the H atom associated with hydroxyl of methanol reacts with the coordinately unsaturated O^{2-} on the ceria surface, resulting in the formation of OH group, as can be observed in Fig. 2. This result is also confirmed by other researchers [31]. The big differences between methanol adsorption on pure ceria and zirconium oxide are the appearance of MMC and the band around 1295 cm^{-1}. Peaks of MMC and 1295 cm^{-1} appear when only CH_3OH adsorbs on ceria catalysts, which cannot be detected on ZrO_2 surface. Based on this result, it is proposed that MMC formation on ceria surface comes from the reaction between methanol and adsorbed CO_2, which is seldom mentioned by other researchers.

When CO_2 is introduced to the ceria catalysts containing preadsorbed methanol, intensity of on-top methoxy which is also considered as the reactive methoxy by other researchers [8, 32] decreases due to the reaction with CO_2. The spectra of CO_2 introduction on zirconium oxide surface after methanol adsorption are similar to earlier reports [33] and agree with the observation that on-top methoxy is more reactive than other types [10]. Noticeably, bands representing for MMC can be both observed on these two catalysts during this CO_2 adsorption process, while the band around 1295 cm^{-1} is only detected on CeO_2. It can be deduced that this band (1295 cm^{-1}) on ceria surface does not originate from single CO_2 adsorption, as shown in Fig. 6. Comparatively, it is noted that the band at 1295 cm^{-1} rises again when the ceria catalyst is exposed to successive introduction of methanol after CO_2 adsorption, further confirming that this band (1295 cm^{-1}) results from the reaction of methanol with adsorbed CO_2.

As can be seen in Fig. 8, features for hydrogen carbonate and monodentate carbonate all decrease during the methanol adsorption on CeO_2 containing preadsorbed CO_2, indicating that

those kinds of adsorbed CO_2 may be involved in the reaction with methoxy. These structures lead to CO_2 activation. The specific reactive structure of CO_2 is not exhibited in this paper because the activated structures depend on the type of oxygen vacancies, crystal face and the coverage of CO_2. It is unreliable to propose the specific structure merely from the results of infrared spectra. The corresponding DFT calculation is in progress.

Further investigation is conducted to decide whether this band (1295 cm^{-1}) represents an intermediate or not. It is a common phenomenon that features for DMC are hard to be observed under the operating experiment condition due to its low concentration. However, according to the theory of microreversibility, a compound decomposition should go through the same elementary steps as it forms. Based on this concept, the DMC decomposition would reveal the intermediate which is needed to produce DMC. The decomposition of DMC on ZrO_2 surface is shown in Fig. 11. Features for MMC and methoxy appear in the adsorption process without the band around 1295 cm^{-1}. So, MMC is the intermediate in DMC formation over zirconium surface. When CeO_2 is exposed to DMC, the band about 1295 cm^{-1} and features for carbonates appear, as observed in Fig. 10. During this process, peaks for MMC are invisible even for a long time exposure, which is much different from the results on ZrO_2. As mentioned above, a band near 1295 cm^{-1} originates from the reaction between methoxy and CO_2 instead of the single adsorption. Depending on the result of DMC adsorption and the theory of microreversibility, it is concluded that peak at 1295 cm^{-1} must be an important feature standing for the intermediate in DMC formation from CO_2 and methanol on CeO_2 surface, meaning that there is a different mechanism in DMC formation on ceria catalysts.

The band about 1295 cm^{-1} has not been assigned so far, but some helpful hints contribute to the definition of this band. Li [29] *et al*. observed a band near 1300 cm^{-1} and associated this band with the ν_s(OCO). Combining the characteristic of this reaction with the band representing

ν_s(OCO), we propose that this band may be the feature of carbomethoxide (CH_3OCO). In order to testify this assumption, methyl formate adsorption is conducted on CeO_2 surface. It is noted that the weak band around 1295 cm^{-1} (1291 cm^{-1}) appears, as observed in Fig. 13. It is probable that appearance of the band about 1295 cm^{-1} comes from methoxy and formate because esters easily decompose into alcohols and carboxylic acids. So, HCOOH adsorption on CeO_2 is applied to verify whether the band about 1295 cm^{-1} stems from formic acid adsorption or not. As exhibited in Fig. 12, bands for ν_s(OCO) appearing at 1353 and 1248 cm^{-1} are far from 1295 cm^{-1}, indicating that it is hard to set up a connection between the band about 1295 cm^{-1} and formic acid adsorption. Moreover, the HCOOH formation from methanol on the surface of ceria is unfavorable under the experiment condition [34], further demonstrating that this band does not come from formic acid adsorption. During the methyl formate adsorption process, it is also noted that there are no features for on-top methoxy, which is well accepted as the reactive methoxy in carbomethoxide formation. Hence, the rising band around 1295 cm^{-1} in methyl formate adsorption process does not result from the reaction between methoxy and CO_2. Then appearance of the band around 1295 cm^{-1} can be explained as follow. The C-H bond that the corresponding C atom links with two oxygen atoms may break up to form H atom and $–OCOCH_3$. The H atom can react with the OH on CeO_2 surface. And the remaining part ($-OCOCH_3$) may attach to the ceria atom on the surface, resulting in the emerging of peak around 1295 cm^{-1}. Although methyl formate adsorption on ceria surface is not a direct evidence of assignment about the new band at 1295 cm^{-1} in DMC formation, it can explain this result to some extent.

Thus, the mechanism of DMC formation directly from CO_2 and methanol over CeO_2 catalyst is described as below, which is different from that previously suggested by other researchers [8, 14]. In this mechanism, CO_2 adsorb on CeO_2 surface to produce adsorbed CO_2 noted as CO_2-CeO_2, as shown in Reaction (1). Reaction (2) is about the adsorption of methanol on ceria

surface. The carbomethoxide forms through the interaction between the adsorbed CO_2 and methanol as depicted in Reaction (3). Methoxy will react with the –C=O in CO_2 to form carbomethoxide. The remaining oxygen atom of CO_2 combines with the hydrogen from the hydroxyl in methanol to produce hydroxyl on the surface of CeO_2. Then the carbomethoxide reacts with another methanol to produce DMC which can be seen in Reaction (4). The formation of carbomethoxide is also strongly supported by the decomposition of DMC.

$$CO_2 + CeO_2 \longrightarrow CO_2\text{-}CeO_2 \quad (1)$$

$$CH_3OH + CeO_2 \longrightarrow CH_3OH\text{-}CeO_2 \quad (2)$$

$$CH_3OH\text{-}CeO_2 + CO_2\text{-}CeO_2 \longrightarrow CH_3OCO\text{-}Ce + OH\text{-}Ce \quad (3)$$

$$CH_3OCO\text{-}Ce + OH\text{-}Ce + CH_3OH \longrightarrow (CH_3O)_2CO + H_2O + CeO_2 \quad (4)$$

Conclusions

The mechanism of DMC formation directly from methanol and CO_2 catalyzed by CeO_2 was investigated, compared with that obtained over ZrO_2. Based on the results of *in-situ* FTIR, DMC formation from CO_2 and methanol over ceria catalyst is proposed to go through a new and different mechanism from that on ZrO_2. On ZrO_2 surface, DMC is formed by the reaction of monodentate methyl carbonate with methanol. Differently, on ceria surface, methanol reacts with the adsorbed CO_2 to produce a new intermediate, carbomethoxide. Feature of carbomethoxide is observed around 1295 cm^{-1}, which is defined through the adsorption of methyl formate. Then DMC is formed via the reaction between carbomethoxide and methoxy coming from the dissociation of methanol. DMC decomposition is observed to experience the reversing way of this route, further confirming that the formation of DMC directly from CO_2 and methanol through carbomethoxide intermediate.

Acknowledgements

Financial support by Natural Science Foundation of China (NSFC) (Grant No. 21176179), the Program for New Century Excellent Talents in University (NCET-13-0411), the Scientific Research Foundation for the Returned Overseas Chinese Scholars (MoE), the Program of Introducing Talents of Discipline to Universities (B06006) is gratefully acknowledged.

References:

1. M. Aresta, A. Dibenedetto and A. Angelini, *Chem. Rev.*, 2013, **113**, 1709-1742.
2. W. Wang, S. Wang, X. Ma and J. Gong, *Chem. Soc. Rev.*, 2011, **40**, 3703-3727.
3. Y. Izumi, *Coord. Chem. Rev.*, 2013, **257**, 171-186.
4. N. A. M. Razali, K. T. Lee, S. Bhatia and A. R. Mohamed, *Renewable. Sustainable. Energy Rev*, 2012, **16**, 4951-4964.
5. J.-C. Choi, T. Sakakura and T. Sako, *J. Am. Chem. Soc.*, 1999, **121**, 3793-3794.
6. A. Dibenedetto, C. Pastore and M. Aresta, *Catal. Today.*, 2006, **115**, 88-94.
7. K. Tomishige, T. Sakaihori, Y. Ikeda and K. Fujimoto, *Catal. Lett.*, 1999, **58**, 225-229.
8. Y. Yoshida, Y. Arai, S. Kado, K. Kunimori and K. Tomishige, *Catal. Today.*, 2006, **115**, 95-101.
9. J. Bian, M. Xiao, S. Wang, Y. Lu and Y. Meng, *Catal. Commun.*, 2009, **10**, 1142-1145.
10. K. T. Jung and A. T. Bell, *J. Catal.*, 2001, **204**, 339-347.
11. C. Sun, H. Li and L. Chen, *Energy. Environ. Sci.*, 2012, **5**, 8475-8505.
12. M. B. Gawande, V. D. B. Bonifacio, R. S. Varma, I. D. Nogueira, N. Bundaleski, C. A. A. Ghumman, O. M. N. D. Teodoro and P. S. Branco, *Green. Chem.*, 2013, **15**, 1226-1231.
13. S. Wang, L. Zhao, W. Wang, Y. Zhao, G. Zhang, X. Ma and J. Gong, *Nanoscale*, 2013, **5**, 5582-5588.
14. H. J. Hofmann, A. Brandner and P. Claus, *Chem. Eng. Tech.*, 2012, **35**, 2140-2146.
15. S. Bernal, G. Blanco, J. Gatica, C. Larese and H. Vidal, *J. Catal.*, 2001, **200**, 411-415.
16. Z. Cheng, B. J. Sherman and C. S. Lo, *J. Chem. Phys.*, 2013, **138**, 014702.
17. K. Tomishige and K. Kunimori, *Applied Catalysis A: General*, 2002, **237**, 103-109.
18. H. Lee, S. Park, I. Song and J. Jung, *Catal. Lett.*, 2011, **141**, 1-7.
19. K. D. Parghi, S. R. Kale, S. S. Kahandal, M. B. Gawande and R. V. Jayaram, *Catal. Sci. Tech.*, 2013, **3**, 1308-1313.
20. S. Rousseau, O. Marie, P. Bazin, M. Daturi, S. Verdier and V. Harlé, *J. Am. Chem. Soc.*, 2010, **132**, 10832-10841.
21. C. Binet and M. Daturi, *Catal. Today.*, 2001, **70**, 155-167.
22. D. G. Rethwisch and J. Dumesic, *Langmuir.*, 1986, **2**, 73-79.
23. G. N. Vayssilov, M. Mihaylov, P. S. Petkov, K. I. Hadjiivanov and K. M. Neyman, *J. Phys. Chem. C.*, 2011, **115**, 23435-23454.
24. C. Li, Y. Sakata, T. Arai, K. Domen, K.-i. Maruya and T. Onishi, *J. Chem. Soc., Faraday Trans. 1 F.,*1989, **85**, 929-943.
25. O. Pozdnyakova, D. Teschner, A. Wootsch, J. Kröhnert, B. Steinhauer, H. Sauer, L. Toth, F. Jentoft, A. Knop-Gericke and Z. Paál, *J. Catal.*, 2006, **237**, 17-28.
26. C. Binet, M. Daturi and J. C. Lavalley, *Catal. Today.*, 1999, **50**, 207-225.
27. W. Hertl, *Langmuir*, 1989, **5**, 96-100.
28. K. T. Jung and A. T. Bell, *Top. Catal.*, 2002, **20**, 97-105.
29. C. Li, K. Domen, K.-i. Maruya and T. Onishi, *J. Catal.*, 1990, **125**, 445-455.
30. G. J. Millar, C. H. Rochester and K. C. Waugh, *J. Chem. Soc., Faraday Trans.*, 1991, **87**, 2785-2793.
31. M. M. Natile, G. Boccaletti and A. Glisenti, *Chem. Mat.*, 2005, **17**, 6272-6286.
32. M. Aresta, A. Dibenedetto, C. Pastore, A. Angelini, B. Aresta and I. Pápai, *J. Catal.*, 2010, **269**, 44-52.
33. K. Tomishige, Y. Ikeda, T. Sakaihori and K. Fujimoto, *J. Catal.*, 2000, **192**, 355-362.
34. Z. Wu, M. Li, D. R. Mullins and S. H. Overbury, *ACS. Catalysis.*, 2012, **2**, 2224-2234.

Table.1. Catalytic activity of different catalysts in DMC formation

	ZrO_2	CeO_2
mmol DMC / g cat	0.21	5.34

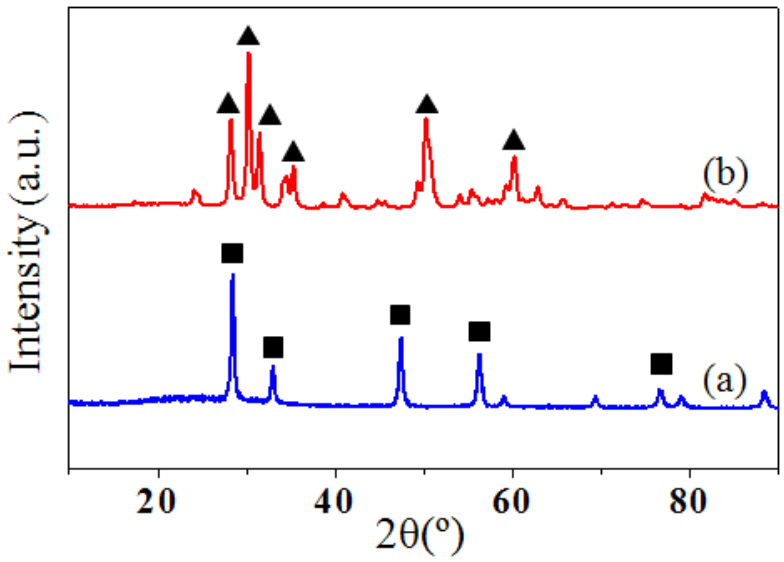

Fig. 1 XRD patterns of different catalysts (a) CeO_2 (b) ZrO_2

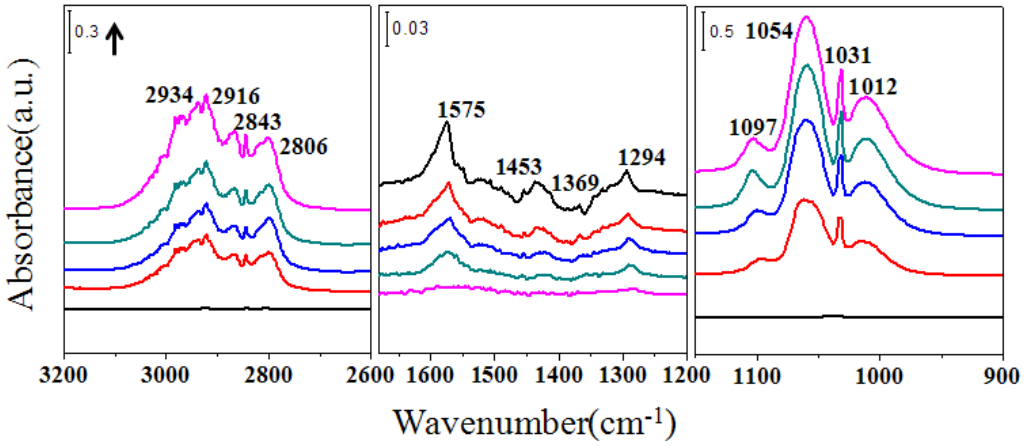

Fig. 2 FTIR spectra of methanol adsorption on CeO_2

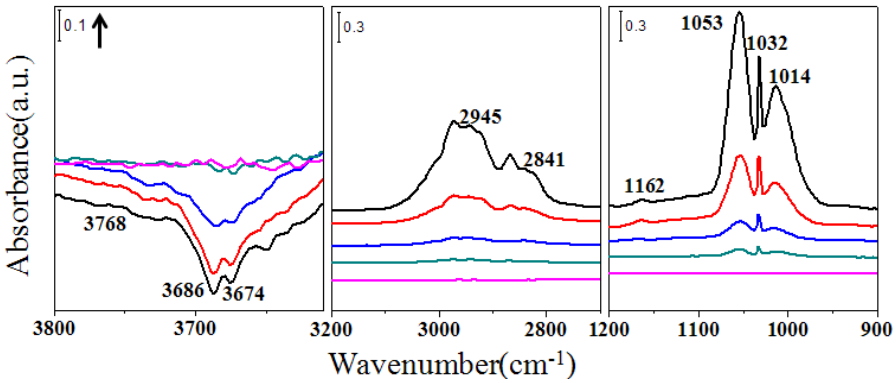

Fig. 3 FTIR spectra of methanol adsorption on ZrO_2

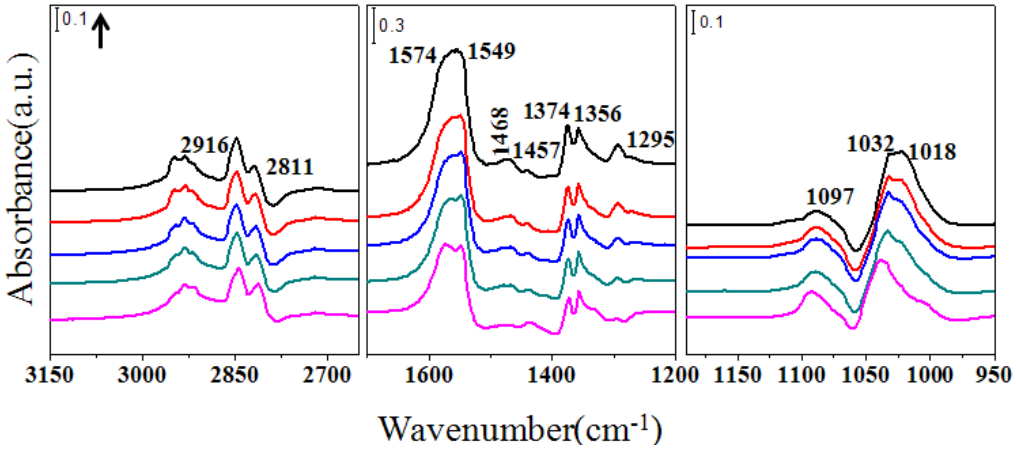

Fig. 4 FTIR spectra of CO_2 successive introduction on CeO_2 after methanol adsorption

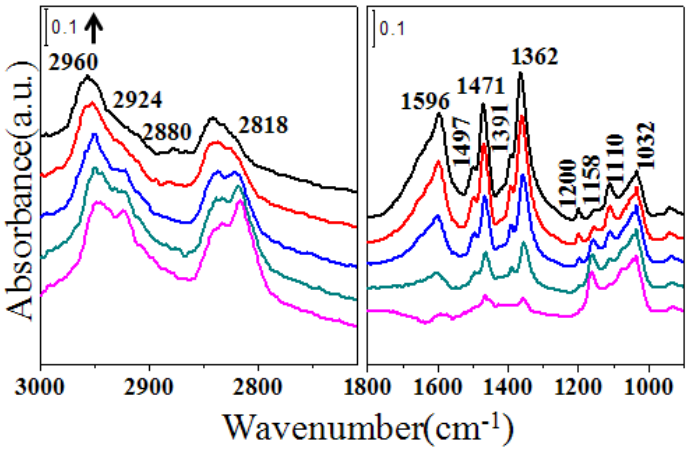

Fig. 5 FTIR spectra of CO_2 successive introduction on ZrO_2 containing preadsorbed methanol

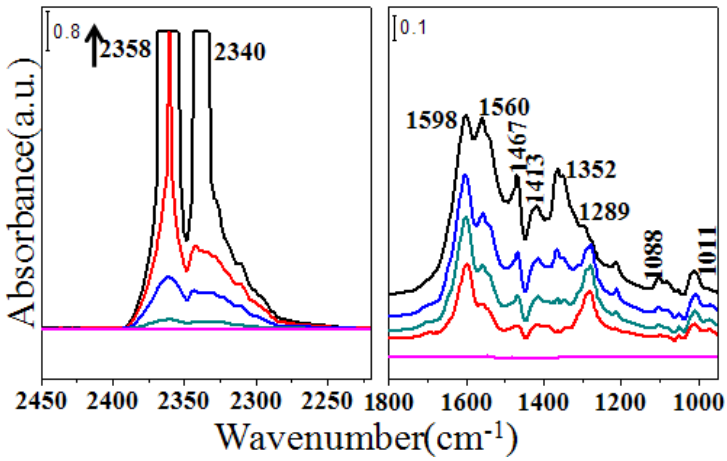

Fig. 6 FTIR spectra of CO_2 adsorption on CeO_2

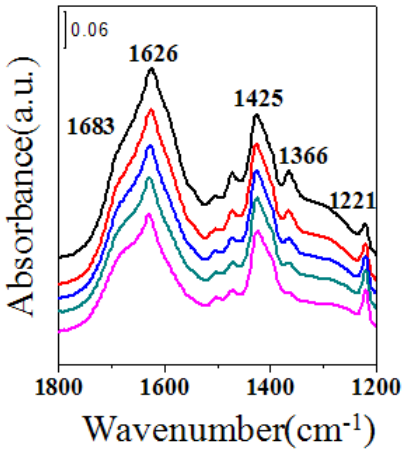

Fig. 7 FTIR spectra of CO_2 adsorption on ZrO_2

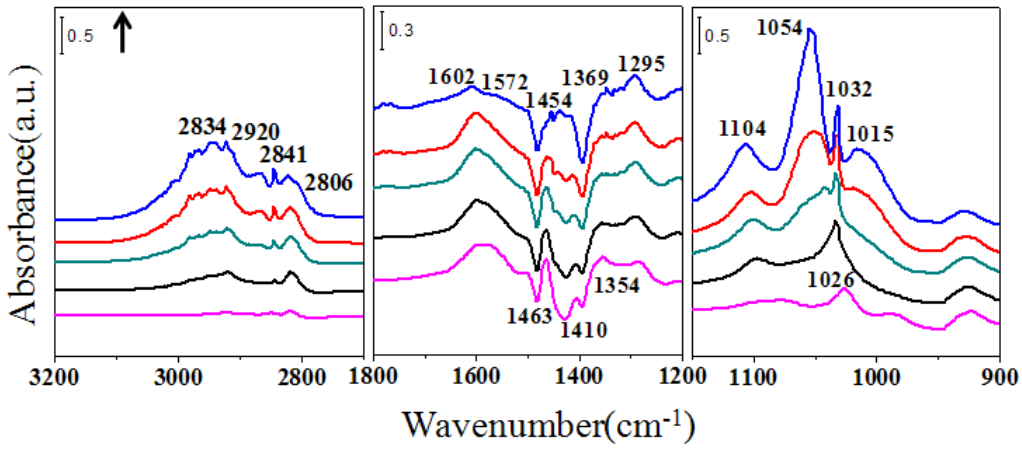

Fig. 8 FTIR spectra of methanol successive introduction to CeO_2 after CO_2 adsorption

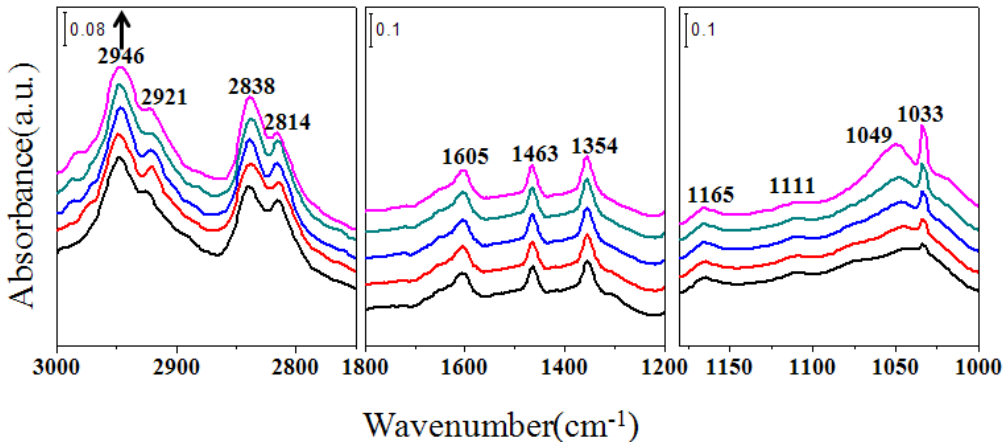

Fig. 9 FTIR spectra of methanol successive introduction after CO_2 adsorption on ZrO_2

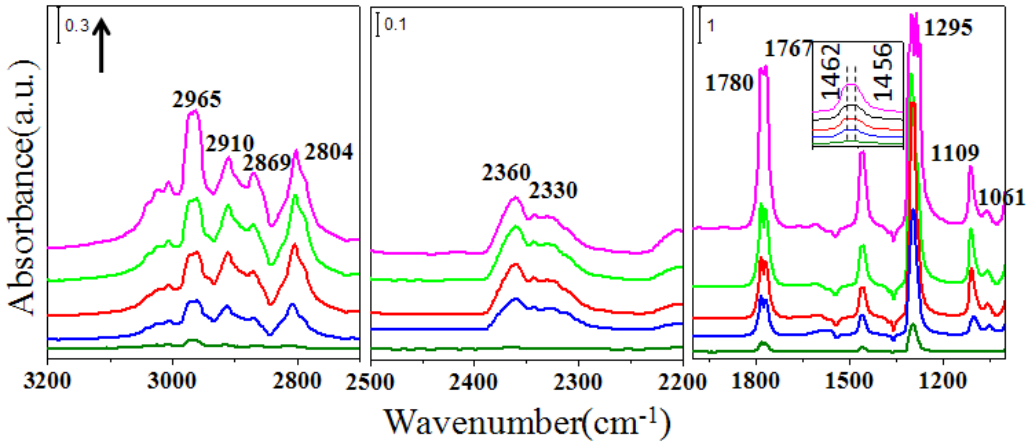

Fig. 10 Infrared spectra of DMC adsorption on ceria catalysts

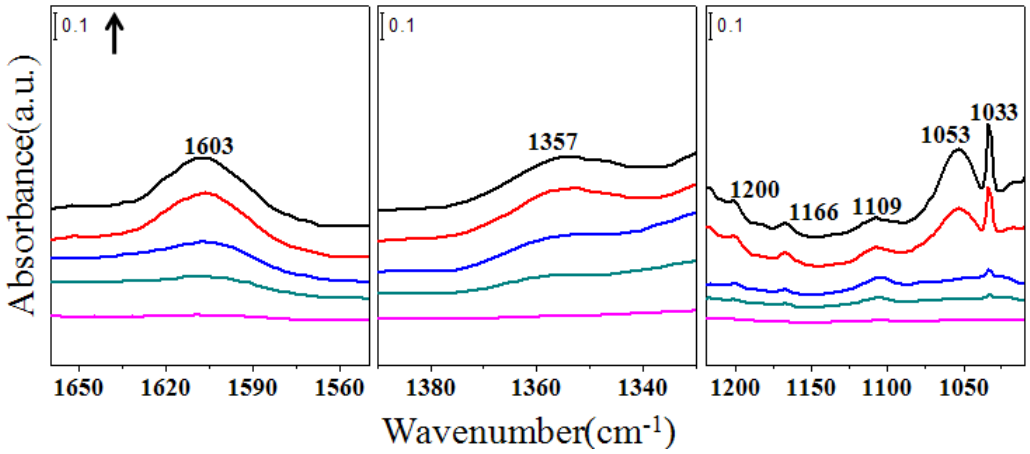

Fig. 11 Infrared spectra of DMC adsorption on zirconium catalysts

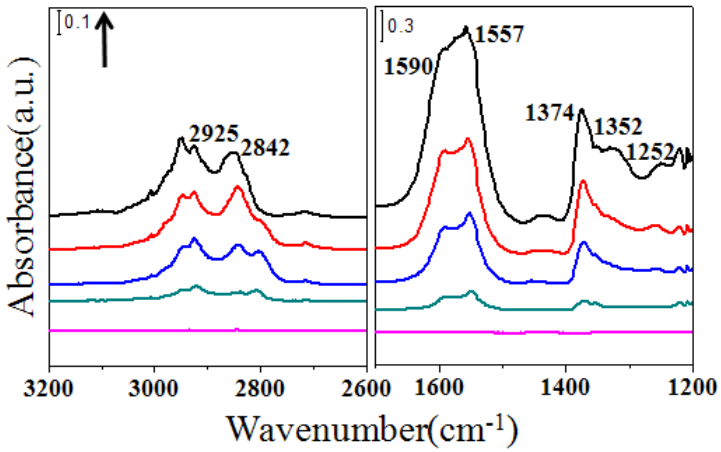

Fig. 12 IR spectra during exposure of CeO_2 to HCOOH

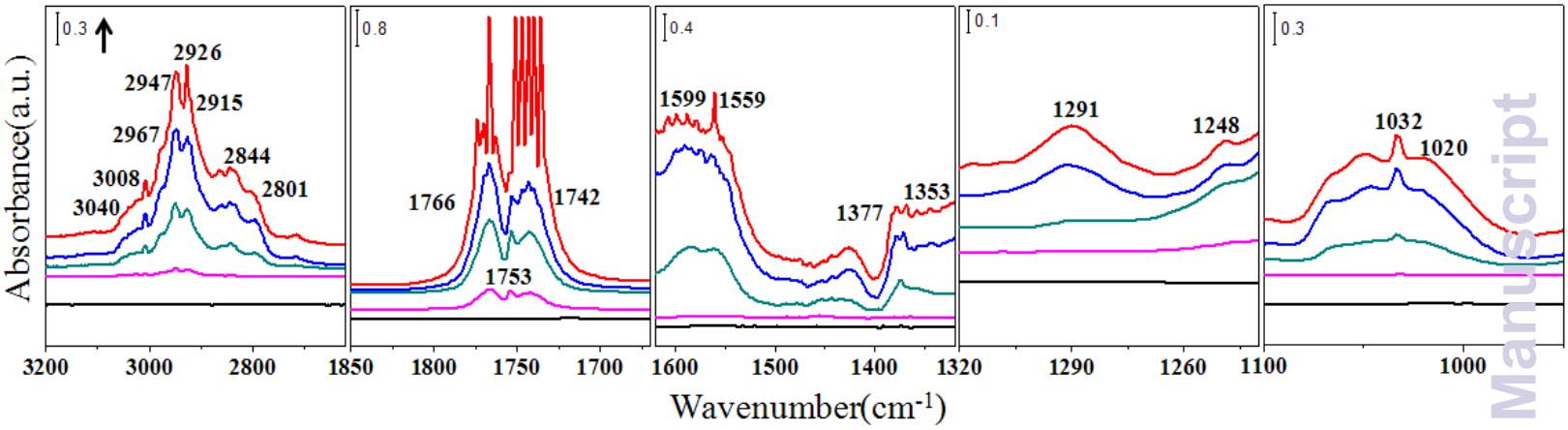

Fig. 13 IR spectra during exposure of CeO_2 to $HCOOCH_3$